Visit **http://www.ravela.net/pinbot.htm** for on-line videos!

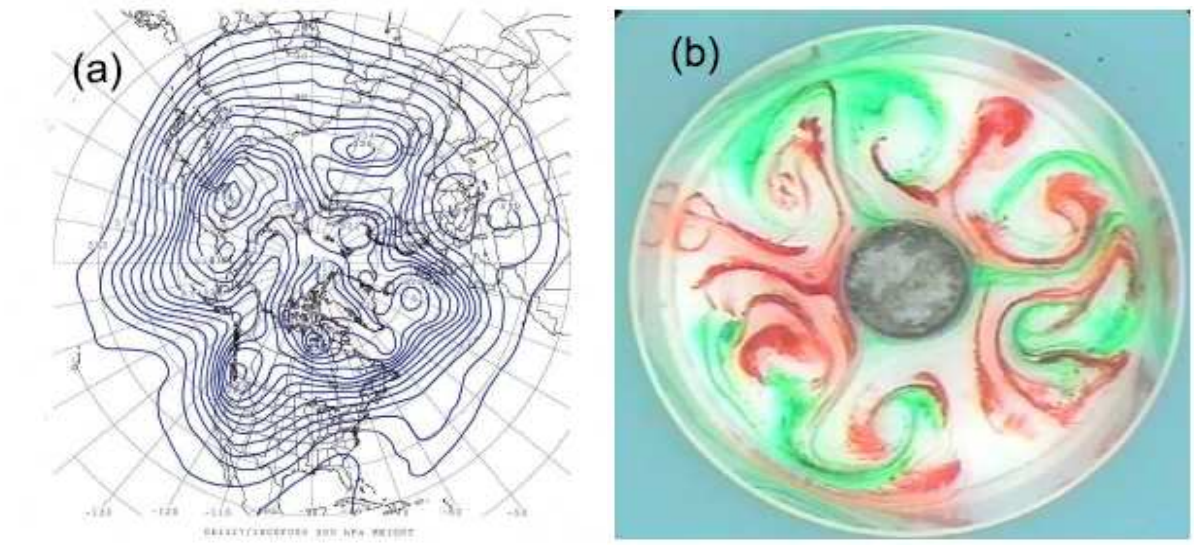

Figure 1. Image (a) shows the 500hPa heights for 11/27/06:1800Z over the northern hemisphere centered at the north pole. Winds flow along the pressure contours. Image (b) shows a tracer (dye) in a laboratory analog. The tank is spinning and the camera is in the rotating frame. Tracer droplets initially inserted at the periphery (red dye, warm region) and around the central chilled can (green dye, cold region) has evolved to form this pattern. The laboratory analog and the planetary system are dynamically akin to one-another. We study the state-estimation problem for planetary flows using the laboratory analog.

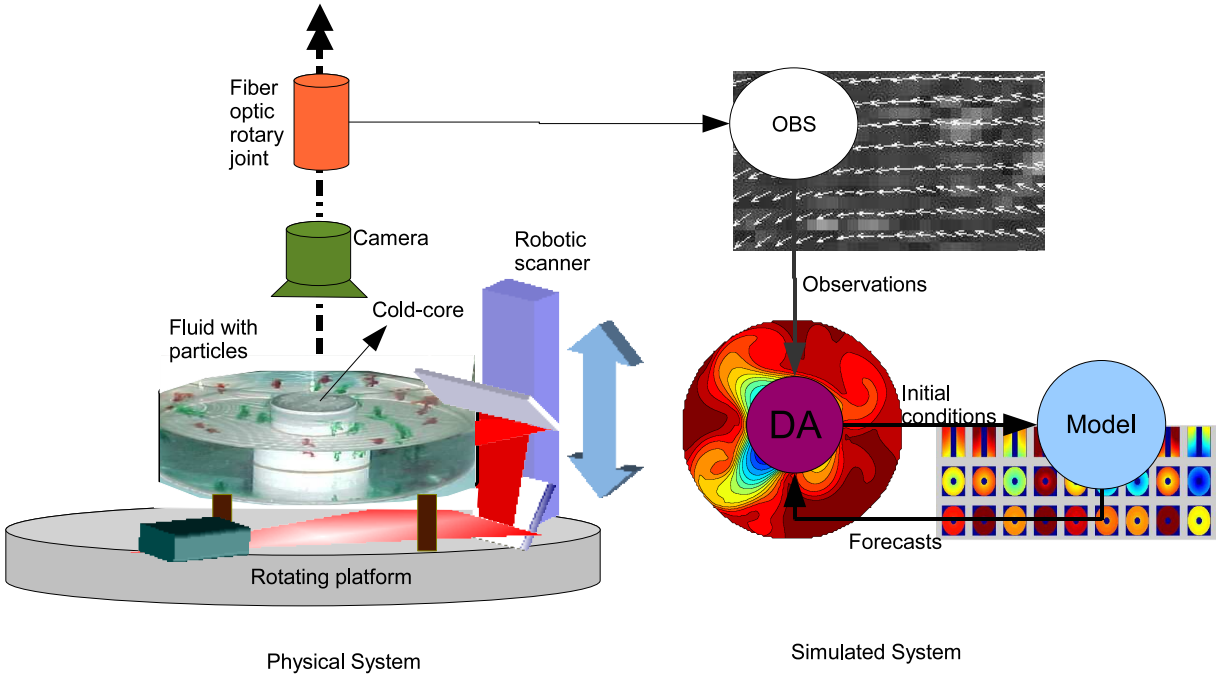

Figure 2. The laboratory observatory consists of a physical system: a rotating table on which a tank, camera and control system for illumination are mounted. The computational part consists of a measurement system for velocimetry, a numerical model, and an estimation system, as described more fully in the text.

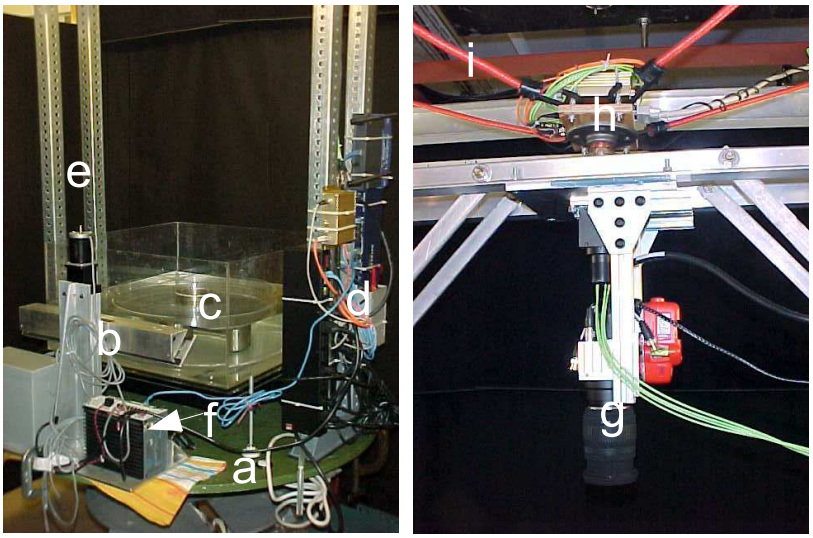

Figure 3. The apparatus consists of (a) the rotating platform, (b) the motorized mirror, (c) the tank, (d) electronics, (e) a rig on which a camera is mounted, (g). Laser light comes from direction (f) and bounces off two mirrors before entering the tank. The fiber optic rotary joint (FORJ) (h) allows images to leave the rotating frame and is held stably by bungee chords (i). The square tank prevents the laser light from bending at the annulus interface.

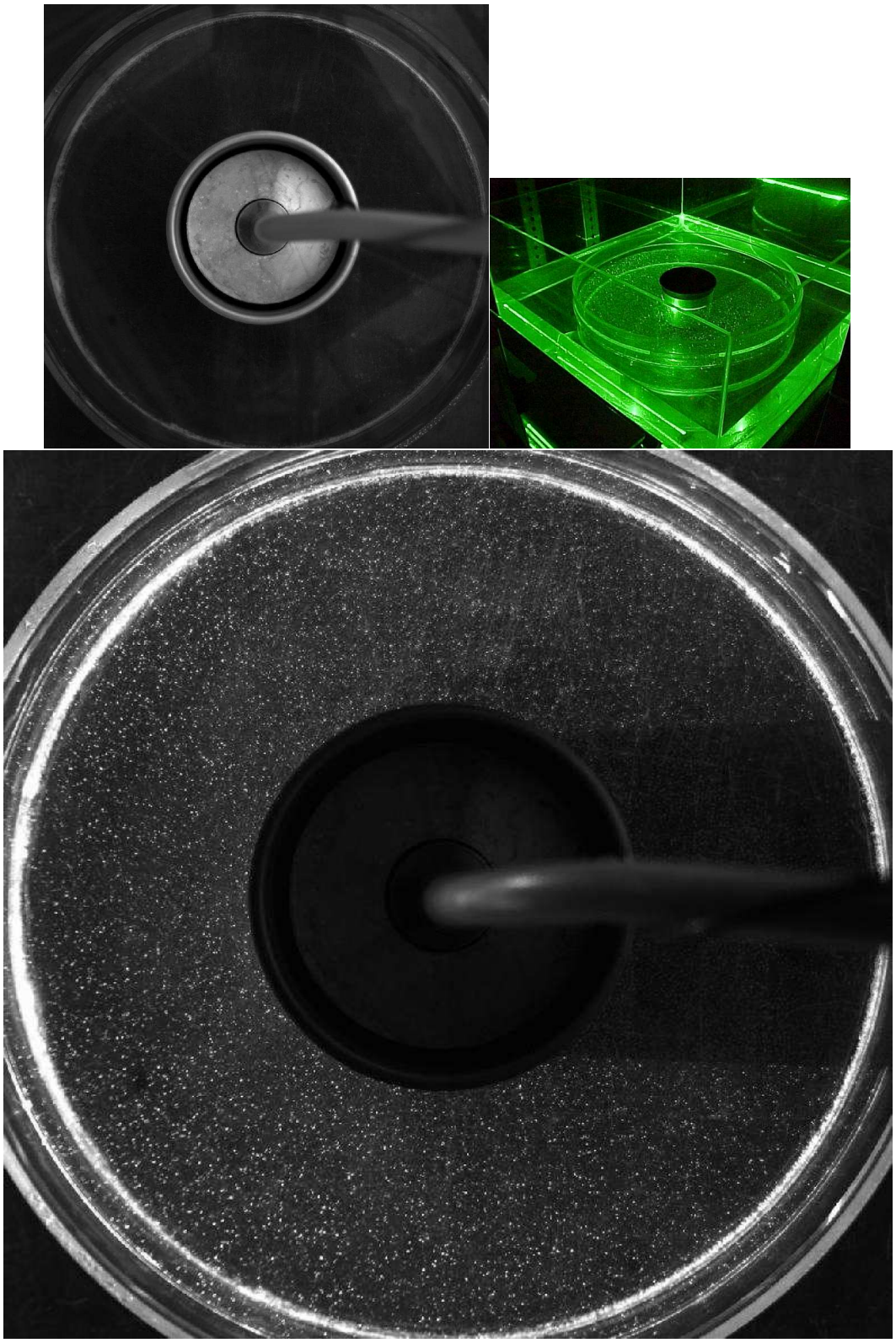

Figure 4. The camera's view of the rotating annulus in visible light (top-left), the laser illuminating the tank (top-right). The camera's view in laser light shows particles (bottom). Notice shadow due to the chiller in the middle. High-resolution version of this figure is in attachment.

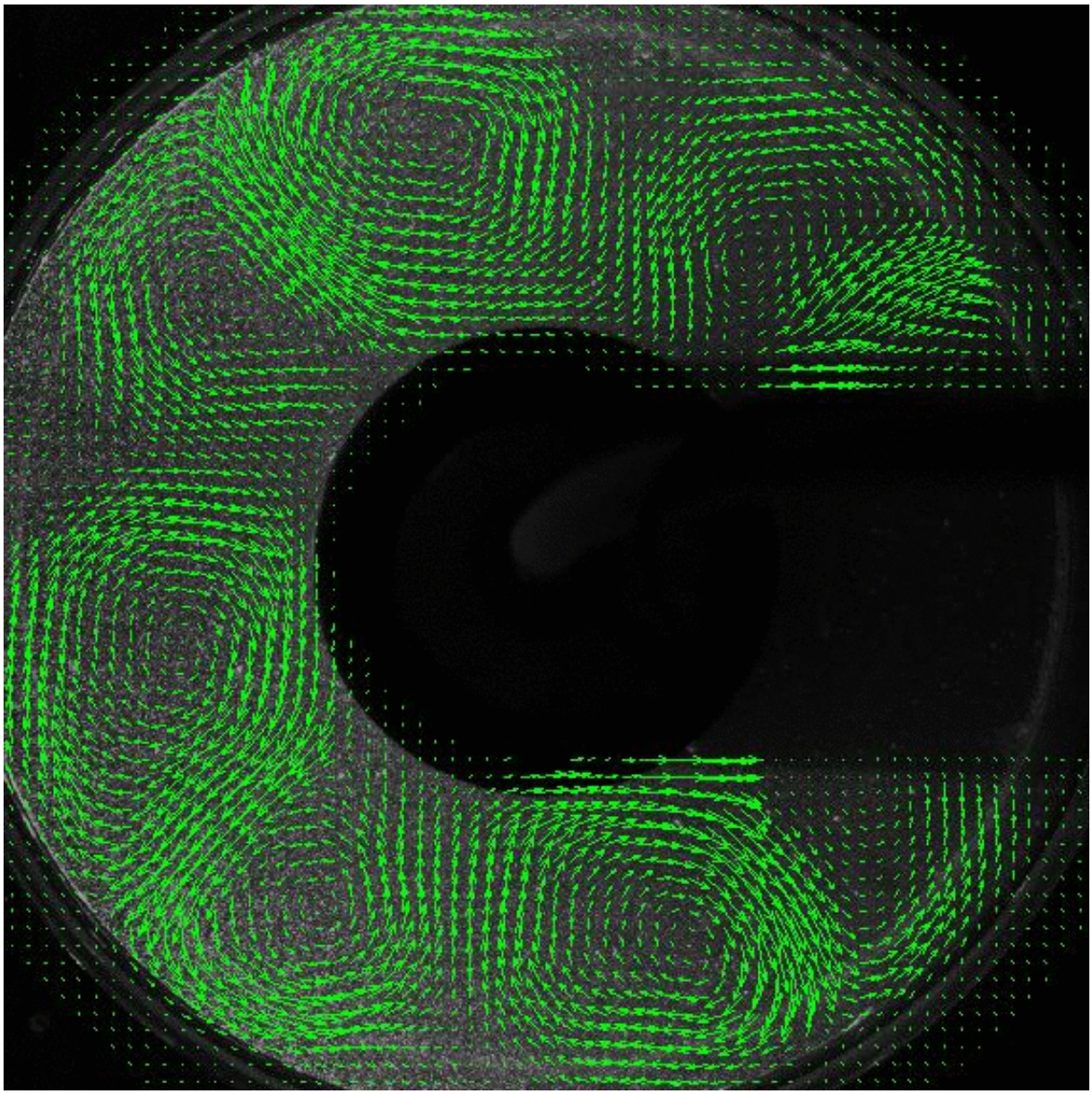

Figure 5. Observed horizontal velocities (green) at $100\ mm$ above the bottom of the tank after circulation has formed. Maximum flow speeds are of the order of $2cms^{-1}$.

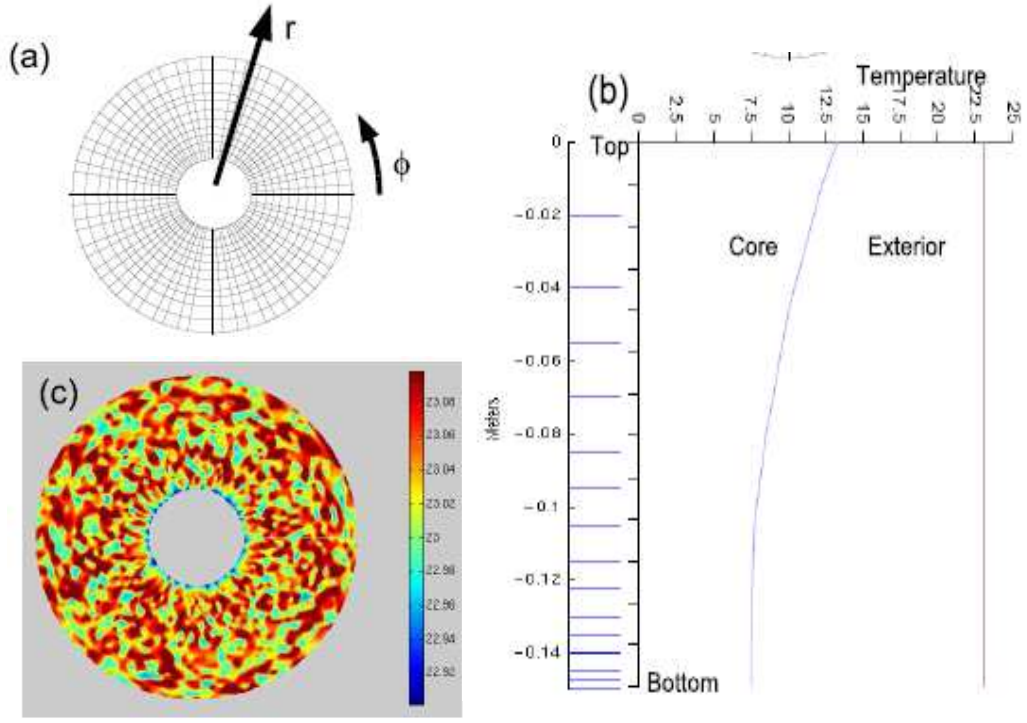

Figure 6. (a) The computational domain is represented in cylindrical coordinates. (b) Depth is discretized with variable resolution to enhance resolution near the bottom-boundary. The lateral boundary conditions on temperature are obtained by interpolating sparse temperature measurements on the boundary. The bottom boundary condition is one of zero heat flux. (c) Random initial conditions are used for the interior temperature field, shown here at a given level.

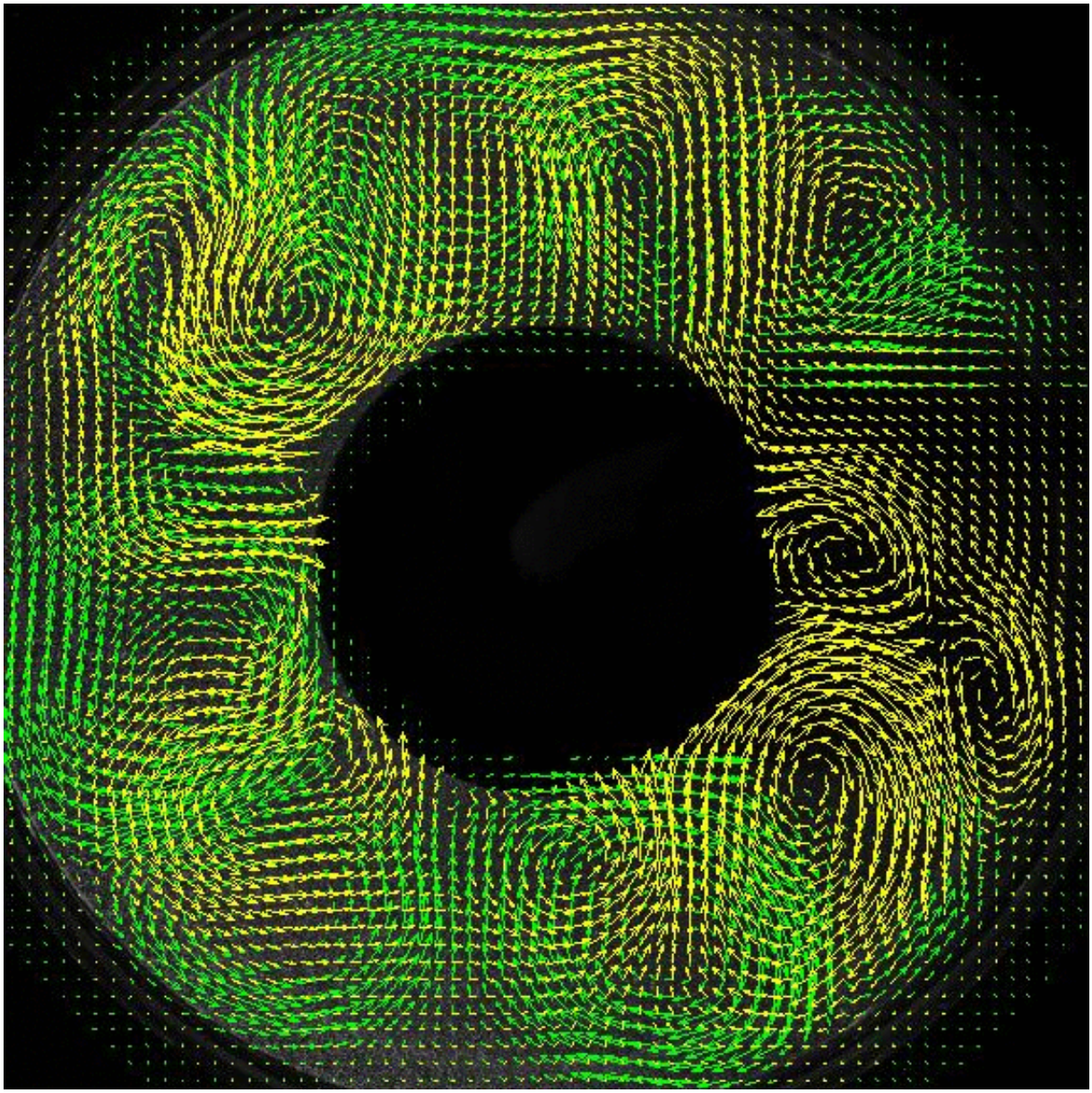

Figure 7. The planar velocity of a model forecast (in yellow) is shown with observed velocity (green) at a height of $100mm$ from the bottom of the tank at the beginning of an estimation experiment. Maximum flow speeds are of order 2 cms^{-1}.

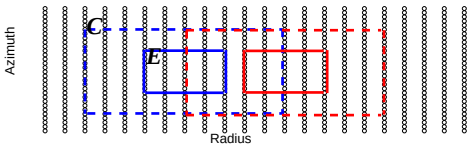

Figure 8. The estimation using the ensemble Kalman filter is localized within estimation windows E, influenced by observations from overlapping spatial-context windows C.

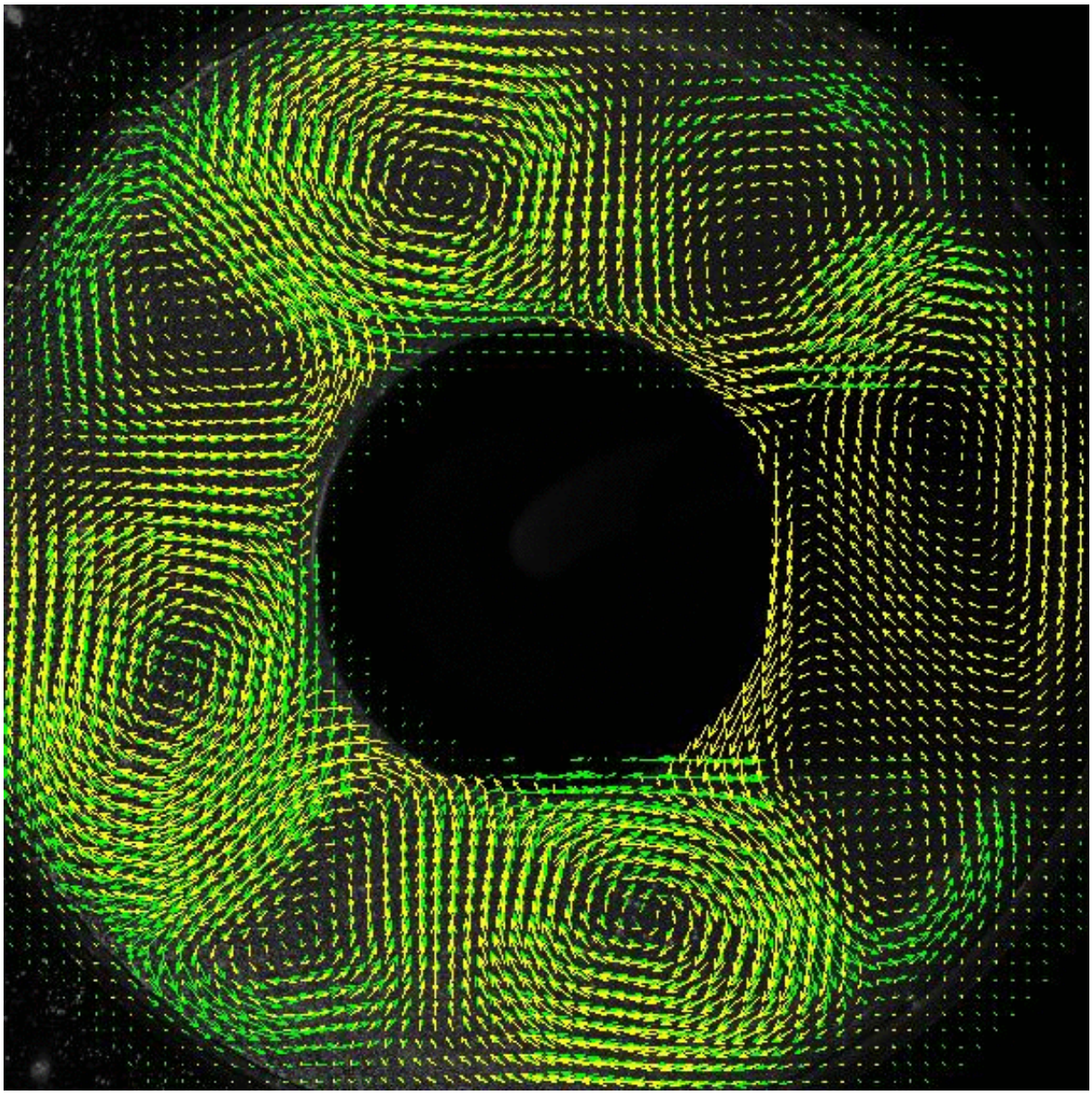

Figure 9. The estimated velocity field at a time $t = 100s$ for an ensemble member at 100mm above the bottom of the tank is shown (yellow). Observations at this layer are shown in (green).

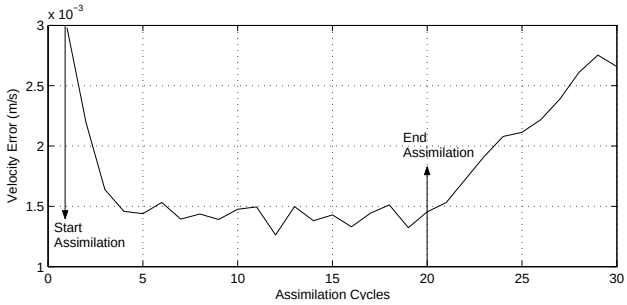

Figure 10. The RMS-error between forecast and observed velocities at all observed locations as a function of time.

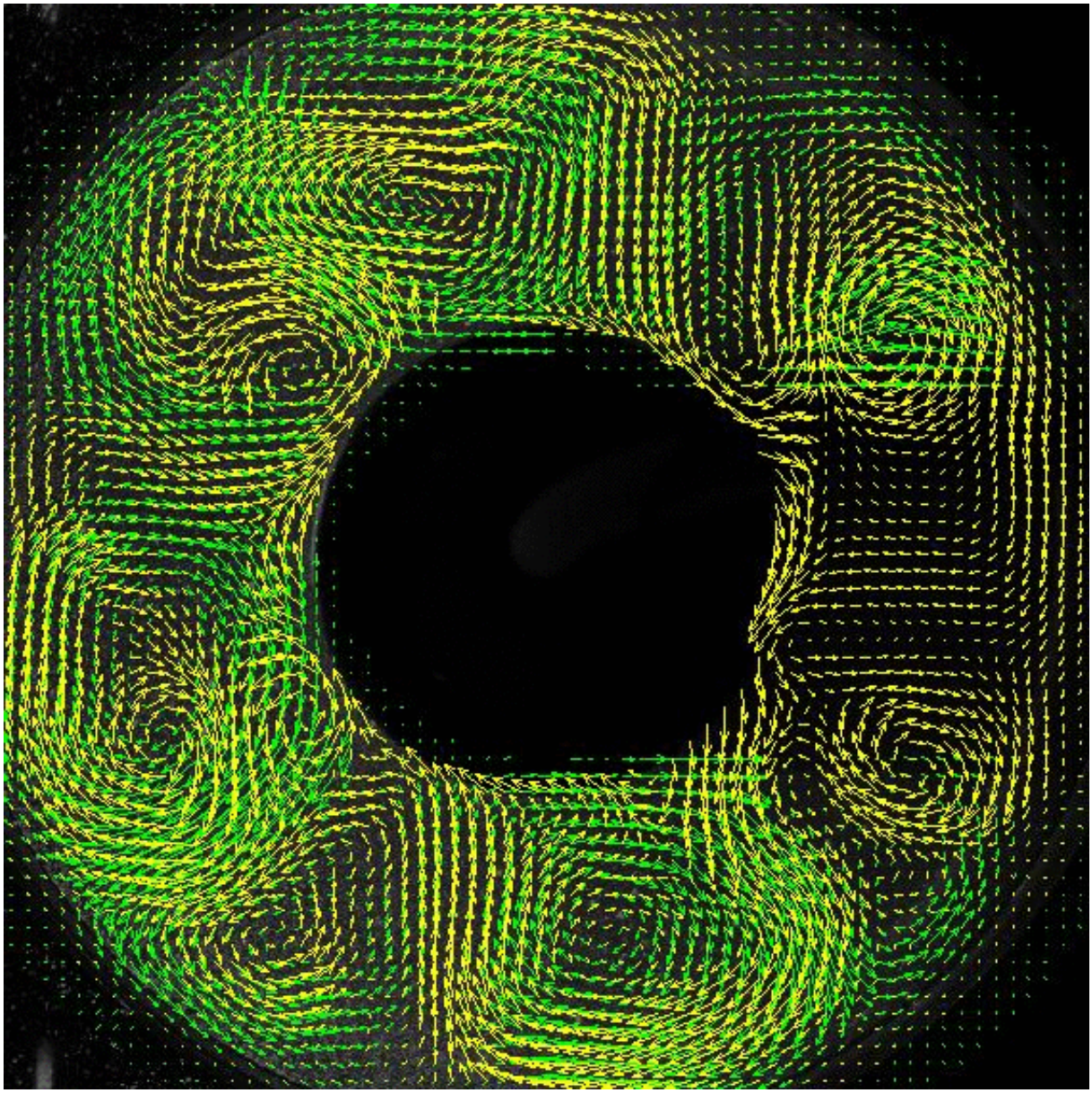

Figure 11. Once filtering is terminated the model diverges from the observations. Shown here is the model velocity for an ensemble member at 100mm above the bottom of the tank (yellow) and corresponding observations (green) at $t = 300s$. NOT IN PAPER